AIChE WILEY InterScience DISCOVER SOMETHING GREAT

MATERIALS, INTERFACES, AND ELECTROCHEMICAL PHENOMENA

Hydrophilic Zeolite Coatings for Improved Heat Transfer: A Quantitative Analysis

Jie Liu and Guillermo Aguilar
Dept. of Mechanical Engineering, University of California, Riverside, CA 92521

Ronnie Munoz and Yushan Yan
Dept. of Chemical and Environmental Engineering, University of California, Riverside, CA 92521

DOI 10.1002/aic.11409
Published online January 24, 2008 in Wiley InterScience (www.interscience.wiley.com).

The wetting diameter and life time of a water droplet on the surface of a bare, ZSM-5 coated, and Zeolite-A coated stainless steel 304 substrate at different initial surface temperatures was experimentally studied. ZSM-5 and Zeolite-A coated SS-304 are more much more hydrophilic than bare stainless steel 304 as reflected by their contact angles (27° and 0° vs. 90°). The ZSM-5 and Zeolite-A coatings significantly outperformed the bare SS-304 by decreasing the droplet life time, increasing the heat flux and increasing the heat transfer coefficient at all initial surface temperatures studied. At the highest surface temperature studied, T_0 = 200°C, ZSM-5, and Zeolite-A coatings are shown to increase the maximum heat flux on bare SS-304 by as much as 106% and 72%, respectively. At this temperature, the maximum heat transfer coefficients on ZSM-5 and Zeolite-A coatings are improved by 470% and 530% over the bare SS-304, respectively. © 2008 American Institute of Chemical Engineers *AIChE J,* 54: 779–790, 2008

Keywords: zeolite coating, hydrophilic, metal, heat transfer, porous

Introduction

Efficient heat exchangers, condensing or evaporative, are critical to numerous industrial processes and practical devices. The central function of many heat exchangers is the extraction or injection of the latent heat from or to liquid water that, in general, can be enhanced by a hydrophilic coating on the metallic heat exchanging surface as a result of improved water contact and spreading.[1–4] For a fin-tube condenser, another benefit of the increased surface hydrophilicity of the fins is a decreased pressure drop.[5] In most fin-tube heat exchangers the distance between the fins is very narrow. As water condenses on the fins, the resulting droplets and bridging water begin to reduce the cross-sectional area for air flow, leading to increased pressure drop and blowing cost. A hydrophilic surface causes the contacting water droplets to spread into a thin film. This film helps to reduce the pressure drop of the air forced through the system, decreases the operation noise and the pumping cost.

Another major consideration for a heat exchanger is metal corrosion.[6–10] Galvanic coatings, and more recent plasma vapor deposition (PVD) coatings, have been used for corrosion protection.[11] The galvanic coatings, however, have negative environmental impact.[11,12] PVD coatings have proved to be promising environmentally friendly alternative for galvanic coatings. If a thick PVD coating is desired for corrosion protection, however, a thin galvanic undercoat often precedes the PVD to help alleviate the relatively high internal stress of the coating. This high stress can cause adhesion problems, but the additional process means that the environmental advantages are partially lost. Additional limitations are often imposed by the size and increased operational cost of the vacuum reactor required for PVD.

Correspondence concerning this article should be addressed to G. Aguilar at gaguilar@engr.ucr.edu and Y. Yan at Yushan.Yan@ucr.edu.

It is evident that coatings that are both hydrophilic and corrosion resistant are desirable.[13] We have demonstrated that zeolite coatings can offer high adhesion and excellent corrosion resistance and they can be easily applied on surfaces of complex shape and in confined spaces by a single-step, environmentally benign, in-situ crystallization process.[11,14–18] In addition, by studying water droplet evaporation on a hot surface, we have shown that zeolite coatings are highly hydrophilic and can improve heat transfer. However, our previous heat transfer study[4] was only semi-quantitative and had limited scope (e.g., only focusing on the water droplet life without the calculation of heat flux and heat transfer co-efficient). It is the goal of this current study to present a much more detailed and quantitative analysis of the heat transfer in a much better controlled experiment.

There have been previous studies that focused on various issues that affect the heat transfer between a water droplet and a sessile surface, such as contact angle,[19] surface roughness,[20] temperature,[21,22] and surfactants.[23,24] However, all of these studies have been performed using direct imaging analysis to obtain the heat transfer characteristics between the water droplet and the sessile surface by assuming that the temperature of the testing surface is constant. However, Zeolite-A coating has very low heat conductivity (~1 W/m.K) and thus the sessile surface temperature may vary significantly during the contact and evaporation of the water droplet. Thus, in this study, we use both direct imaging and a computational heat transfer technique to study: (a) spread dynamics of a water droplet in contact with three different surfaces: SS-304, ZSM-5, and Zeolite-A preheated to three different initial temperatures, *x*, *y*, and *z*°C; (b) overall spread and life time of each droplet; and (c) surface temperature and heat flux time variations during the droplet spreading and evaporation processes. To overcome the problem of varying surface temperature, the surface temperature variation was measured directly and an Inverse Heat Conduction (IHC) algorithm[25,26] was used to calculate the heat flux between the water droplet and the sessile surface. The direct imaging analysis obtained from the high speed video was used as an auxiliary approach only.

Experimental

Surface preparation: application of coatings to a single side of the substrate

Two SS-304 mirror finished panels measuring 7.62 × 15.24 × 0.061 cm^3 were sandwiched together using a high temperature epoxy along the edges. The epoxy was allowed to cure at room temperature for two days. The sandwiched panels were cleaned by submersion for 20 min in 1 N HNO_3 at 21°C. The sandwiched panels were rinsed under de-ionized water and dried with compressed air. The purpose of this procedure was to deposit zeolite coating only on one side of the metal panels.

The synthesized ZSM-5 solution contained a molar composition of 0.16 TPAOH: 0.64 NaOH: 1 TEOS: 92 H_2O: 0.0018 Al (TPAOH is tetraproplyammonium hydroxide and TEOS is tetraethylorthosilicate). A typical solution preparation began with the addition of 0.0126 g aluminum powder (200 mesh, 99.95+%, Aldrich) to 100 g double de-ionized water. Then 6.33 g sodium hydroxide (pellets, 97+%, Aldrich) was added to the solution and stirred for 30 min. To this solution, 297.03 g double de-ionized water and 20.12 g TPAOH (40 wt %, Sachem) were then added and stirred for 30 min. Finally 51.5 g TEOS (98 wt %, Aldrich) was added to the solution and stirred for 4 h. The sandwiched panels with 1500 ml of ZSM-5 synthesis solution were placed vertically into a large 2,000 ml sealed Teflon lined autoclave (Parr Instrument Co.) and heated in a convection oven at 175°C for 12 h. The coated sandwiched panels removed from the autoclave were rinsed with de-ionized water and dried with compressed air. The sandwiched panels were then cut using an industrial shear into single side coated substrates measuring 2 × 3.5 × 0.061 cm^3.

The Zeolite-A synthesis solution contained a molar composition of 10 NaOH: 0.2 Al_2O_3: 1 SiO_2: 200 H_20. A typical solution preparation began with the addition of 1.182 g aluminum powder (200 mesh, 99.95+%, Aldrich) to 364.4 g double de-ionized water. Then 87.5 g sodium hydroxide (pellets, 97+%, Aldrich) was added to the solution and stirred for 30 min. To this solution, 21.9 g Ludox® LS30 colloidal silica (30 wt %, silica, Aldrich) was added to the solution and stirred for 4 h. The sandwiched panels with 1500 ml of Zeolite-A solution were placed vertically into 2000 ml polypropylene bottle and heated in a convection oven at 65°C for 12 h. The coated sandwiched panels removed from the polypropylene bottle were rinsed under de-ionized water and dried with compressed air. The sandwiched panels were then cut using an industrial shear into single side coated substrates measuring 2 × 3.5 × 0.061 cm^3.

Characterization of coated and uncoated substrates

The application of a ZSM-5 coating onto a single side of the SS-304 mirror-finished substrate surface was verified using X-ray diffraction (XRD, Siemens D-500 diffractometer using Cu K_α radiation) and scanning electron microscope (SEM, Philips XL30-FEG operated at 20 kV). The same was done for the Zeolite-A coated substrate.

The wettability of the coated and uncoated surfaces was determined by contact angle measurements (VCA Optima XE). A 28-gauge blunt tip needle was attached to a VCA Optima XE mechanically controlled micrometer for dispensing a 2 μl double de-ionized water droplet onto the surface of a sample. Twelve contact angle measurements were taken on the center of the sample, which was then dried with compressed air so that the measurement could be repeated. Twenty-four measurements were made on the surface of the three samples and the averages and standard deviations were obtained for the collected data.

Characterization of boiling dynamics and heat transfer

The setup used to conduct the heat transfer experiments and observe the droplet evaporation is shown in Figure 1. A uniform heating surface was constructed for the heat transfer experiments using a 7.6 × 7.6 × 0.2 cm^3 fiberglass reinforced silicone-rubber 90 watt heating blanket (3) sandwiched between a 7.6 × 7.6 × 2.54 cm^3 copper block (4) and a 8.3 × 8.3 × 1.3 cm^3 piece of silica board insulation (2). One 0.1-mm thick fast response thin foil CEMENT-ON® thermocouple (5) (Omega Engineering, Inc) was attached to the back of the substrates testing surface (10). A 0.2 mm

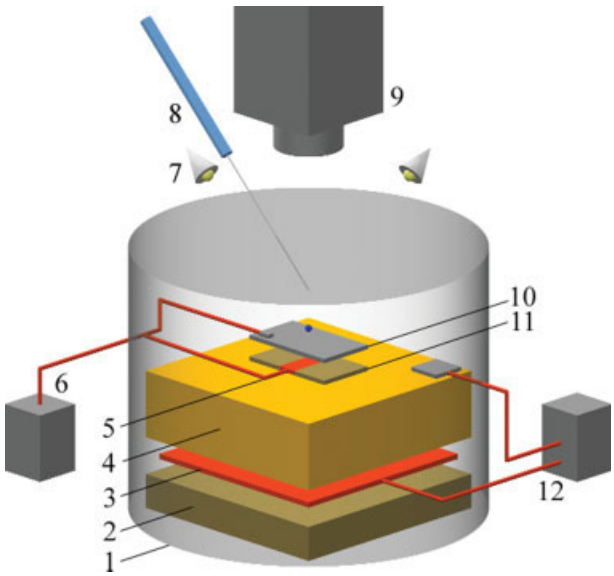

Figure 1. Experimental Setup.

(1) Acrylic cover, (2) Silica board insulation, (3) Heating Blanket, (4) Copper Block, (5) Thin Foil Thermocouple, (6) Acquisition Unit, (7) Illumination, (8) Precise Micro-liter Syringe, (9) High Speed Camera, (10) Testing Surface, (11) High Heat Conductivity Thermal Epoxy and (12) PID Heat Controller. [Color figure can be viewed in the online issue, which is available at www.interscience.wiley.com.]

thick OMEGABOND-200® high heat conductivity epoxy adhesive (11) (Omega Engineering, Inc) was used to bond and reduce the thermal resistance between the testing and heated surface. The temperature variation was recorded by an Instrunet® (Omega Engineering, Inc) fast data acquisition system (6) set at 1000 data points per second. Usually, in order to measure the surface temperature and heat flux between the droplet and the sessile surface, the thermocouple is directly attached to the surface, but in this study, attaching the thermocouple on the surface would affect its hydrophilic and heat transfer characteristics. To avoid this problem, the temperature was measured underneath the testing surface. The heat flux and heat transfer coefficient on the upper surface may then be calculated by using the measured temperatures at the bottom, and an IHC technique.[25] Considering that the testing surface is only 0.6-mm thick and that the length and width of the thermocouple (0.5×0.5 mm^2) are much less than those of the testing surface, the 2D heat conduction scenario may be simplified to a 1D problem.[25] This means that the calculated results stand for the heat transfer characteristics between the testing surface and water droplet.

This experimental approach allows us to study, for the first time, the dynamics of droplet spreading and evaporation phenomena simultaneously, which are both affected by the hydrophilic nature of the sessile surfaces. The key feature of this experimental design is that the initial and boundary conditions for all experiments and surfaces are identical, and by looking at the transient behavior (both wetting/drying and heat transfer) of a droplet gently deposited on the surface, it is possible to discern the effect between impermeable surfaces (SS) and the unique porous hydrophilic ones (ZSM-5 and Zeolite-A) on the liquid spreading and evaporation. This is in contrast with classical pool boiling tests, which not only require a strict control of either the temperature or heat flux at the surface, but they can only provide information about the surface heat transfer and not about the spreading and filtering. Furthermore, an important parameter to evaluate the hydrophilicity of the surfaces is the contact angle between the water droplet and sessile surface.[4] Using a single droplet heat transfer experiment, we can also directly associate the heat flux at the surface with the static contact angle, which would not be possible in a pool boiling experiment.

A 90-mm zoom lens (V-HQ Macro MC 90 mm f/2.5, Elicar, Japan) high speed camera (9) (Photron Fastcam PCI 10K, Itronics, Westlake Village, CA) was used to acquire the digital images of a water droplet boiling on the three different surfaces. Two Fiber-Lite illuminators (7) (Edmund Industrial Optics, Barrington, NJ) were placed above the testing surfaces. The camera was positioned directly above and vertical to the horizontal test surface. The entire heating surface was placed within an Acrylic cylinder (1) to limit convection currents and fixed on top of an adjustable stage to allow horizontal leveling of the testing surface. The initial temperature at the copper block surface (upon which the samples were placed) was controlled by a PID temperature controller (12) capable of maintaining the temperature of the samples to within $\pm 1^\circ$C of the set point. A precise micro-liter syringe (7) was used to gently deposit a water droplet with constant volume of 7.4 μl onto the testing surfaces.

Results and Discussion

Both ZSM-5 and Zeolite-A coatings showed their respective standard diffraction patterns (Figure 2). The presence of a continuous and well intergrown polycrystalline zeolite coating for both ZSM-5 and Zeolite-A was verified by SEM (Figure 3a, c). The coating thickness for ZSM-5 and Zeolite-A was examined by exposing the profile of the coating to a hydrofluoric acid etch (Figure 3b, d) and determined to be about 4.5 μm.

The contact angle for the SS-304 mirror finished substrate was $90.2 \pm 1.4^\circ$ (Figure 4). For ZSM-5 coated SS-304, the contact angle was $27.3 \pm 5.1^\circ$. Upon placing a drop on the

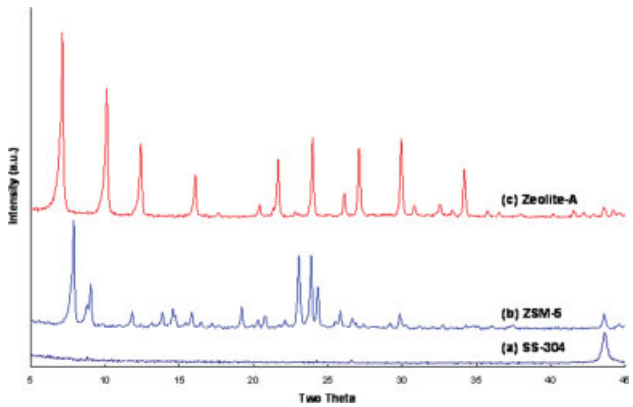

Figure 2. X-ray diffraction patterns of (a) SS-304, (b) ZSM-5 coated SS-304, and (c) Zeolite-A coated SS-304.

[Color figure can be viewed in the online issue, which is available at www.interscience.wiley.com.]

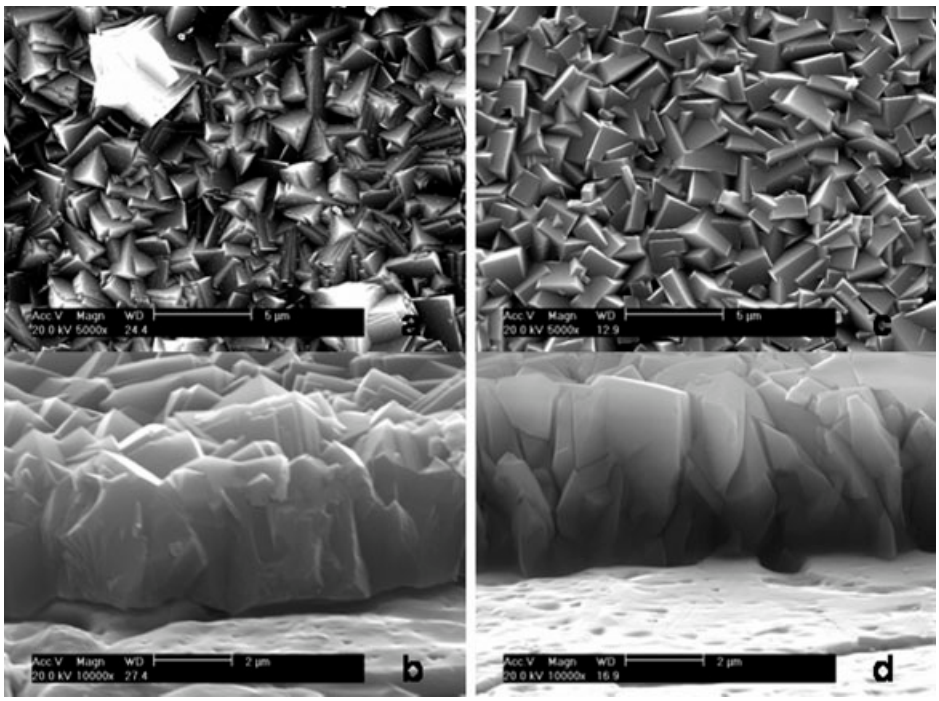

Figure 3. SEM images of top (a,c) and cross sectional (b,d) views of: Zeolite-A on SS-304 (a,b) and ZSM-5 on SS-304 (c,d).

Films are ~5 m thick.

surface of a Zeolite-A coated substrate, the drop was wicked away so quickly that the contact angle was difficult to obtain and was approximated as zero°.

Figure 5 shows the water droplet boiling images at T_0 = 130°C for SS-304, ZSM-5, and Zeolite-A surfaces. Once the water droplet contacts the surface, the whole process can be distinguished as five consecutive stages: Stage I, initial contact; II, wetting area developing; III, maximum wetting; IV, end of boiling; and V, dry-out. For SS-304, from initial contact to the maximum wetting (Stages I–III: 0–1.624 s), the wetting area remains approximately unchanged with an average wetting diameter of about 4 mm. The dry-out process (Stage V) is slow, taking more than 8 s. A small bulk of the water can be observed during the whole dry-out process. For the ZSM-5 surface, the wetting area increases with time while major bubbles are observed during the boiling process. At 1.064 s, two large bubbles can clearly be seen in the droplet that reaches a maximum wetting diameter of 7.5 mm. During the dry-out, no bulk water is observed and eventually non-wet areas can be observed clearly due to the bubble growth during the boiling process. For the Zeolite-A surface, the droplet undergoes rapid spreading while numerous tiny bubbles grow and explode in its interior. It reaches a maximum wetting diameter of 13 mm at 0.112 s, and during the dry-out, the wetting diameter is the largest of the three surfaces.

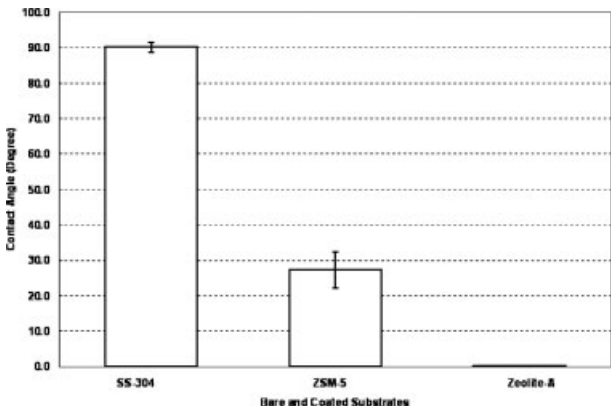

Figure 4. Wetting angle measurements on (a) SS-304, (b) ZSM-5 coated SS-304, and (c) Zeolite-A coated SS-304.

Figure 6 shows the water droplet boiling images at T_0 = 160°C for SS-304, ZSM-5, and Zeolite-A surfaces. The boiling phenomena for a water droplet on SS-304 at T_0 = 160°C are similar to what occurs at T_0 = 130°C. From the initial contact to the maximum wetting (0–0.204 s), the wetting diameter is almost constant at 3.8 mm and splashing is clearly observed during the boiling process. Dry-out begins at 1.440 s and it takes much shorter time than the dry-out process at T_0 = 130°C. For the ZSM-5 surface, the wetting area increases with time and reaches a maximum wetting diameter of about 9.4 mm at 0.196 s. During this boiling process, the bubble size remains smaller than that at T_0 = 130°C, and thus the non-wetting area during the dry-out is smaller than that at T_0 = 130°C. For the Zeolite-A surface, the water droplet begins to boil and spread quickly, and this is similar to the case at T_0 = 130°C. The maximum wetting diameter is smaller than that at T_0 = 130°C, about 9.7 mm at 0.136 s.

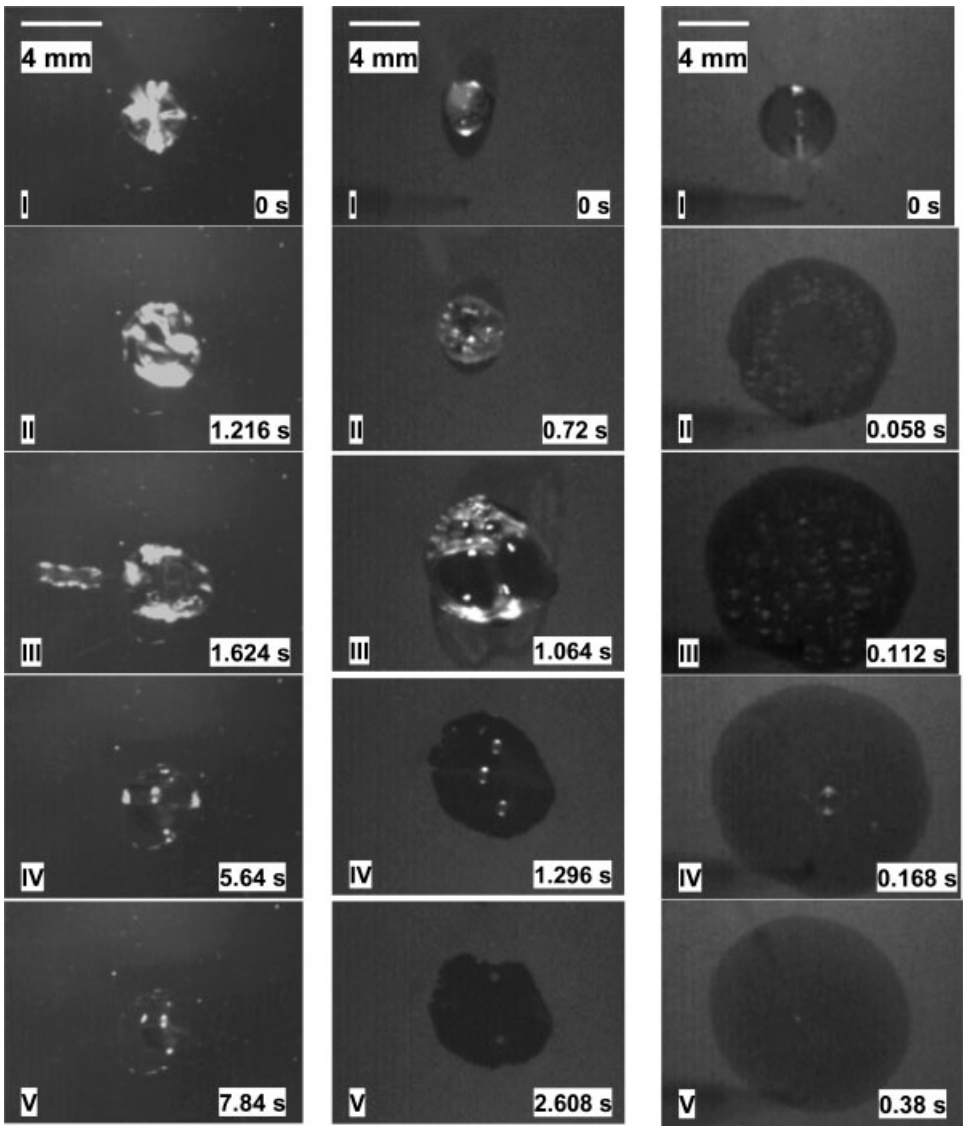

Figure 5. Water droplet evaporation on the testing surfaces: SS-304 (Left column), ZSM-5 (Middle column), and Zeolite-A (Right column).

Images taken at an initial surface temperature of 130°C show the water droplets in their sequential stages: I, Initial contact; II, Wetting area developing; III, Maximum wetting; IV, End of boiling, and; V, Dry out.

The dry-out time remains almost the same as that at T_0 = 130°C.

Figure 7 shows the water droplet boiling images at T_0 = 200°C for SS-304, ZSM-5, and Zeolite-A surfaces. For the SS-304 surface, violent splashes are observed immediately. The bulk of water droplet disappears around 0.100 s. The dry-out process is not observed because there is no water left on the surface after the splash. For the ZSM-5 surface, the droplet spreads rapidly and is characterized by very aggressive boiling. A maximum wetting diameter of 10.8 mm is obtained at 0.046 s. The dry out process is concluded in less than 0.150 s. Unlike the dry-out process at T_0 = 130 and 160°C, there is nonwetting area during the dry-out at T_0 = 200°C. For the Zeolite-A surface, the droplet begins to spread at a rate much slower than those observed for the surface at T_0 = 130 and 160°C. The maximum wetting diameter of 6.7 mm, which is much smaller than that at T_0 = 130 and 160°C, is obtained at 0.194 s .During the dry-out, the wetting area is smaller than that at T_0 = 130 and 160°C.

The wetting diameters of the water droplet during the evaporation process on the three surfaces at different initial temperatures are plotted in Figure 8. The wetting diameter of the droplet on the surfaces of ZSM-5 and Zeolite-A are for the most part significantly larger than that on SS-304, at any given time for the three initial surface temperatures of T_0 = 130, 160, and 200°C. These large droplet diameters are a consequence of the ZSM-5 and Zeolite-A coating's excellent hydrophilicity (Figure 4). The water droplet wetting diameter, with respect to time, does not fluctuate much on the SS-304 surface at the initial surface temperatures of T_0 = 130, 160, and 200°C, but the droplets on ZSM-5 and Zeolite-A surfaces have large changes in their wetting diameters with

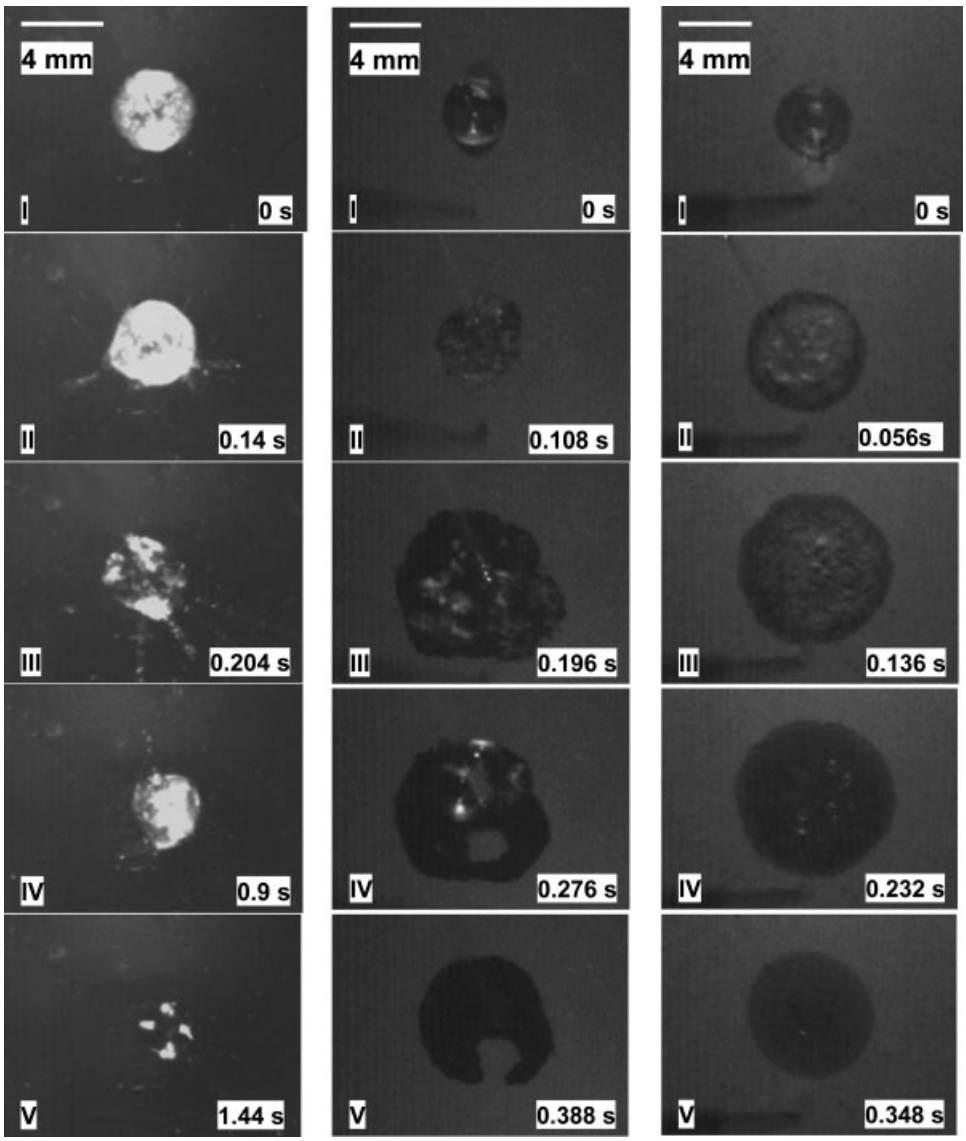

Figure 6. Water droplet evaporation on the testing surfaces: SS-304 (Left column), ZSM-5 (Middle column) and Zeolite-A (Right column).

Images taken an initial surface temperature of 160°C show the water droplets in their sequential stages: I, Initial contact; II, Wetting area developing; III, Maximum wetting; IV, End of boiling, and; V, Dry out.

respect to time for all temperatures studied. For ZSM-5, the maximum wetting diameter increases as the temperature is increased to 200°C while for Zeolite-A, the maximum wetting diameter decreases as T_0 increases.

The maximum wetting diameter depends on two competing and correlated parameters: wettability of the surface and the rate of evaporation. Better wettability tends to increase the diameter of the droplet while faster evaporation tends to decrease the maximum wetting diameter. Note that better wettability originates from a better match of surface energy. It is known that as temperature increases, the surface tension (or energy) of water is reduced, making water much more "spreadable" on a surface with a moderate surface energy (i.e., ZSM-5 surface) and less "spreadable" on Zeolite-A surface. But this should have very little effect on a surface like SS-304 because its surface energy is still too low even for the hot water droplet. For SS-304, as the initial temperature of the surface increases, there is little change for the wettability, but the evaporation rate increases. This is reflected by the slight decrease in the maximum wetting diameter. For the ZSM-5 surface, the wettability increases significantly as the temperature increases and thus much larger maximum wetting diameter is achieved relative to the other two surfaces. In contrast, for the Zeolite-A surface, poorer wettability and faster evaporation work together to lower the maximum wetting diameter as the temperature increases.

The life time of the water droplet on the three surfaces at different temperatures is shown in Figure 9. For SS-304 and ZSM-5, the life time shortens with increasing temperature. This is consistent with the hypothesis that higher temperature increases the rate of evaporation for SS-304 and ZSM-5. For Zeolite-A, however, the life time shortens as the temperature

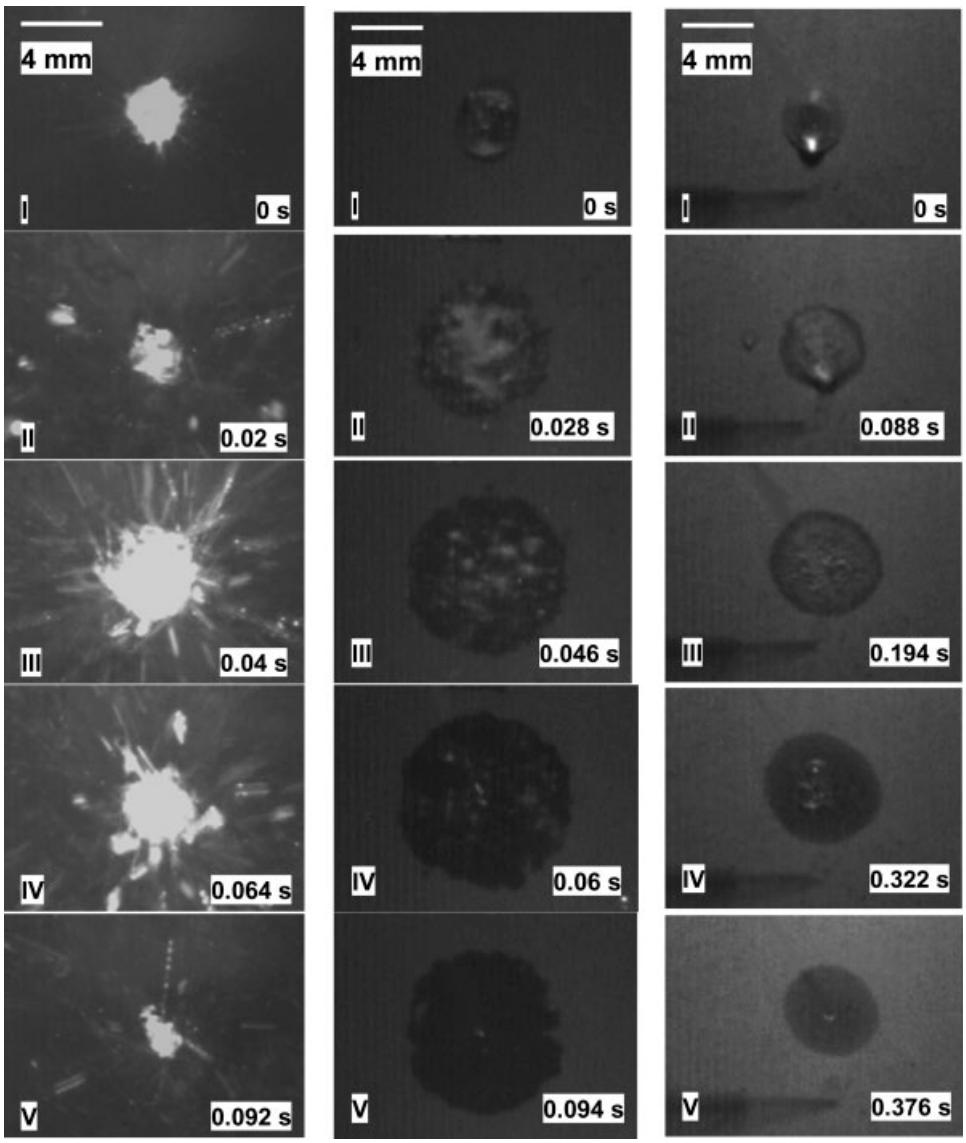

Figure 7. Water droplet evaporation on the three surfaces.

SS-304 (Left column), ZSM-5 (Middle column) and Zeolite-A (Right column). Images taken at an initial surface temperature of 200°C show the water droplets in their sequential stages: I, Initial contact; II, Wetting area developing; III, Maximum wetting; IV, End of boiling, and; V, Dry out.

is increased to 160°C, but any further increase in temperature does not significantly change the life time of the droplet. It is believed that below 160°C, increasing temperature leads to faster overall evaporation, and thus shorter life time. But above 160°C, another factor has to be considered, and that is the microporosity. The ZSM-5 coating has an organic template in its micropores and thus is nonporous, but the Zeolite-A coating has no template in its micropores and thus is microporous. The longer life time of water droplet on Zeolite-A is likely a result of the increased difficulty to drive out the water adsorbed inside the micropores.

Figure 10 shows the calculated surface temperature variation with time. At $T_0 = 130$°C, the lowest temperature that a water droplet at 24°C can cool the surface to is 110, 105, and 102°C for SS-304, ZSM-5, and Zeolite-A, respectively. At this temperature, Zeolite-A decreases the surface temperature the fastest and has the best ability to cool down the surface. For $T_0 = 160$°C, the lowest temperatures that a water droplet at 24°C can cool the surface to is 105°C for both Zeolite-A and ZSM-5, but only to 130°C for SS-304. The rate of decrease in the surface temperatures for ZSM-5 and Zeolite-A are very close at this temperature. For $T_0 = 200$°C, the lowest temperatures that a water droplet at 24°C can cool the surface to is 110°C for both Zeolite-A and ZSM-5, but only to 145°C for SS-304. The rate of decrease in the surface temperature of ZSM-5 is the fastest at this temperature.

Figure 11 shows the surface heat flux variation corresponding to temperature variations described in Figure 10. For $T_0 = 130$°C, the Zeolite-A has the largest heat flux, with a maximum value of 3.3×10^6 W/m^2. The maximum heat flux values for SS-304 and ZSM-5 are 1.8×10^6 W/m^2 and 2.3×10^6 W/m^2, respectively. For $T_0 = 160$ °C, the maxi-

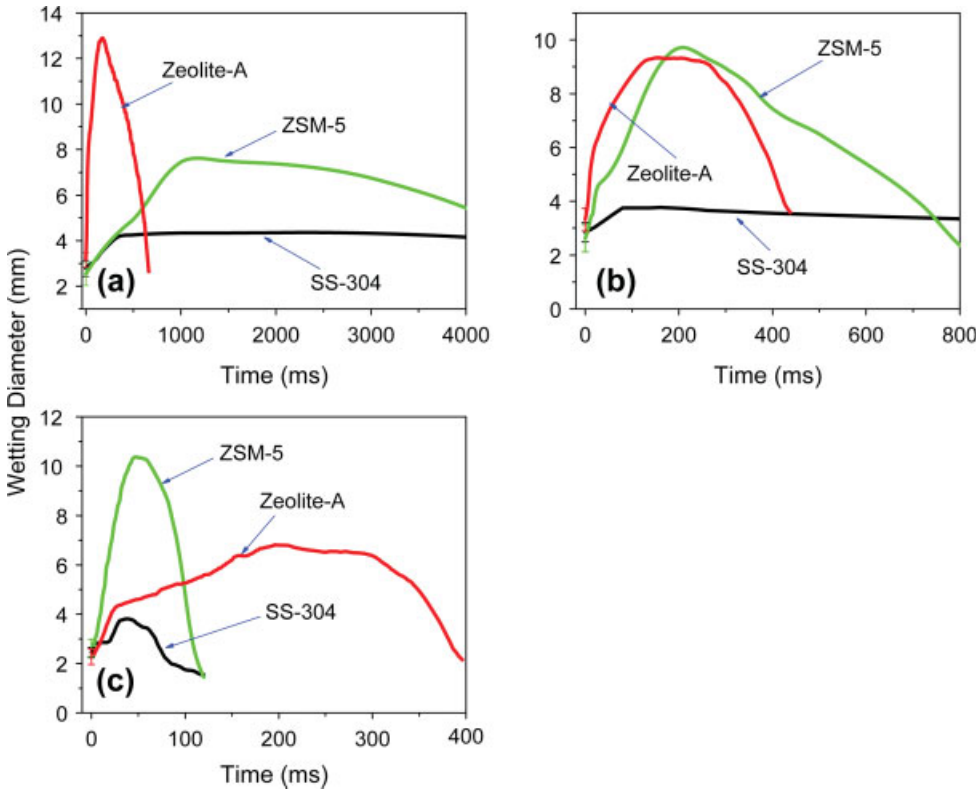

Figure 8. Variation of wetting diameter with time for the three testing surfaces at different surface initial temperatures, T_0.

(a) T_0 = 130°C, (b) T_0 = 160°C, and (c) T_0 = 200°C. [Color figure can be viewed in the online issue, which is available at www.interscience.wiley.com.]

mum heat flux values are 2.7 × 10^6 W/m^2, 4.8 × 10^6 W/m^2, and 4.5 × 10^6 W/m^2 for SS-304, ZSM-5 and Zeolite-A, respectively. For T_0 = 200°C, ZSM-5 has the largest heat flux, with a maximum value of 9.7 × 10^6 W/m^2. The maximum heat flux values for SS-304 and Zeolite-A are 4.7 × 10^6 W/m^2 and 8.1 × 10^6 W/m^2, respectively.

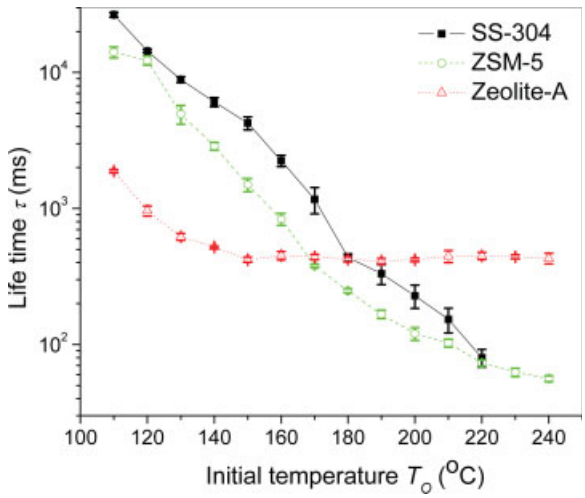

Figure 9. Life time (τ) of a water droplet on the three testing surfaces.

SS-304, ZSM-5, and Zeolite-A, at different surface initial temperatures, *To*. [Color figure can be viewed in the online issue, which is available at www.interscience.wiley.com.]

Figure 12 shows the heat transfer coefficient computed from the surface heat fluxes shown in Figure 11 and using an average droplet temperature. For T_0 = 130°C, the Zeolite-A has the largest heat transfer coefficient, with a maximum value of 6.3 × 10^5 W/m^2 K. The maximum heat transfer coefficients for SS-304 and ZSM-5 are 4.9 × 10^5 W/m^2 K and 1.8 × 10^5 W/m^2 K, respectively. For T_0 = 160°C, the maximum heat transfer coefficients are 1.9 × 10^5 W/m^2 K, 8.0 × 10^5 W/m^2 K and 1.1 × 10^6 W/m^2 K for SS-304, ZSM-5, and Zeolite-A, respectively. For T_0 = 200°C, the maximum heat transfer coefficients are 1.9 × 10^5 W/m^2 K, 1.1 × 10^6 W/m^2 K, and 1.2 × 10^6 W/m^2 K for SS-304, ZSM-5, and Zeolite-A, respectively.

All these calculated heat transfer properties agree well with the image analyses shown in Figures 8–10 and demonstrate that the wettability of a surface affects the boiling phenomenon which in turn affects the heat transfer properties between a droplet and the surface. At T_0 = 130°C, the Zeolite-A demonstrates the best heat transfer performance with a maximum heat flux that is almost 100% and 30% better than the bare SS-304 and ZSM-5. In Figure 5, the large bubbles that appear on the ZSM-5 surface produce vapor that reduces the heat transfer between the hot surface and water droplet. The Zeolite-A surface only has tiny fast breaking bubbles that produce a negligible void.

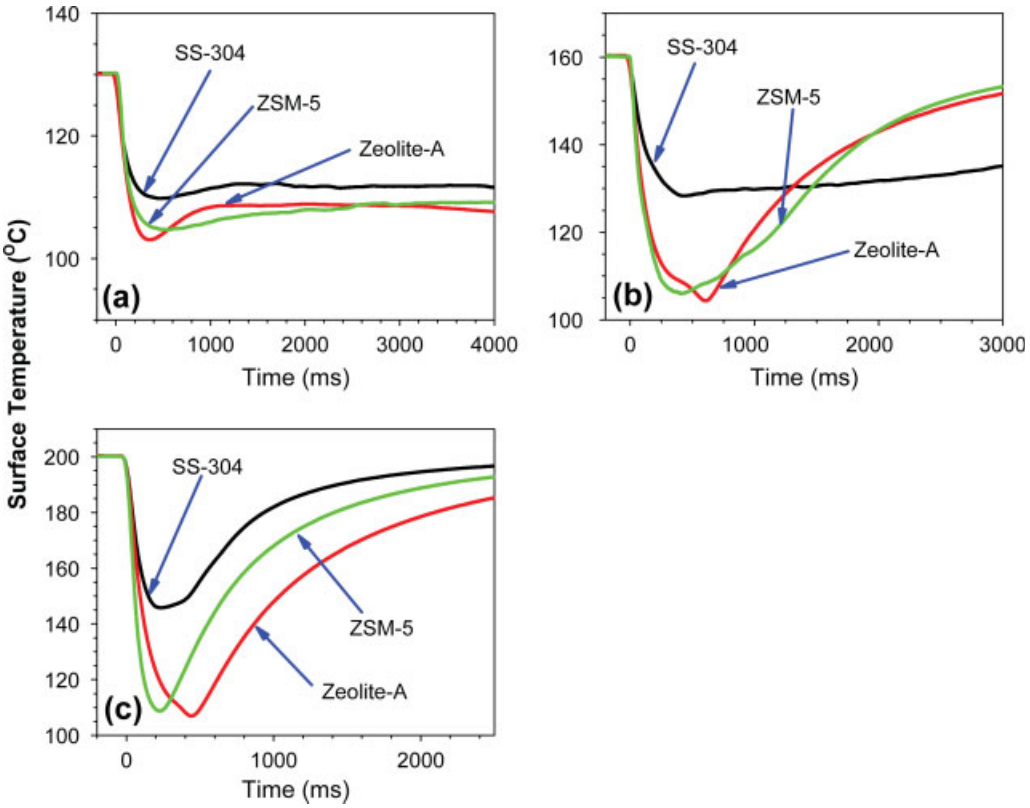

Figure 10. Surface temperature variation with time for different surface initial temperatures T_0.

(a) T_0 = 130°C, (b) T_0 = 160°C, and (c) T_0 = 200°C. [Color figure can be viewed in the online issue, which is available at www.interscience.wiley.com.]

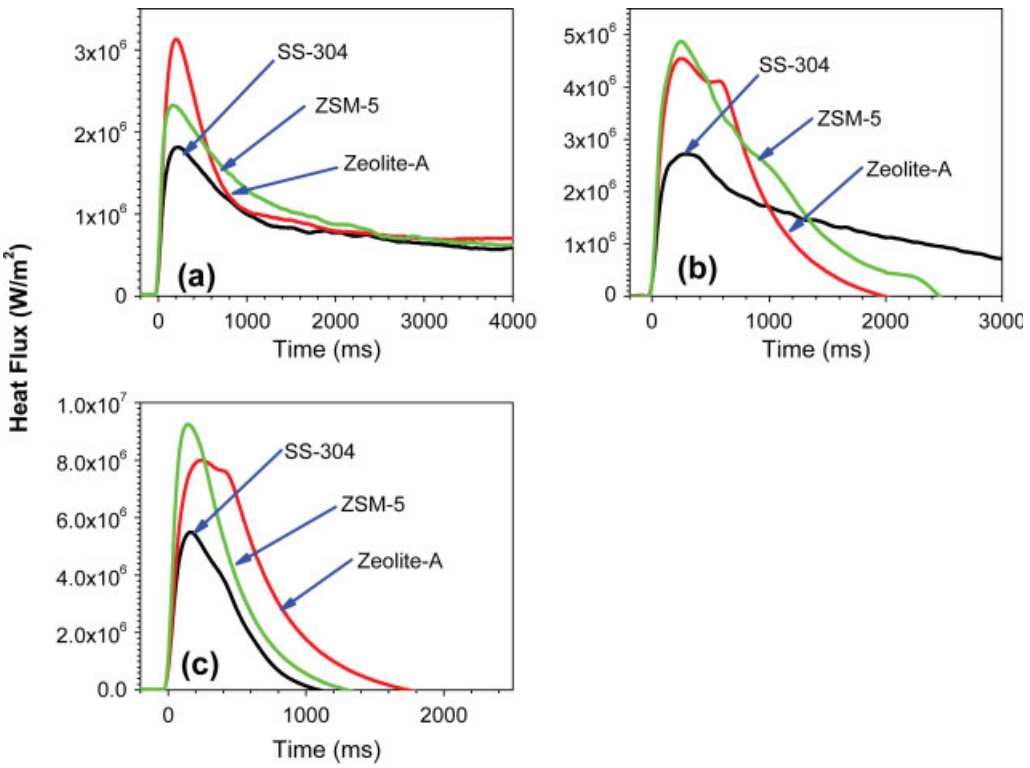

Figure 11. Heat flux (q'') variation with time for different surface initial temperatures T_0.

(a) T_0 = 130°C, (b) T_0 = 160°C, and (c) T_0 = 200°C. [Color figure can be viewed in the online issue, which is available at www.interscience.wiley.com.]

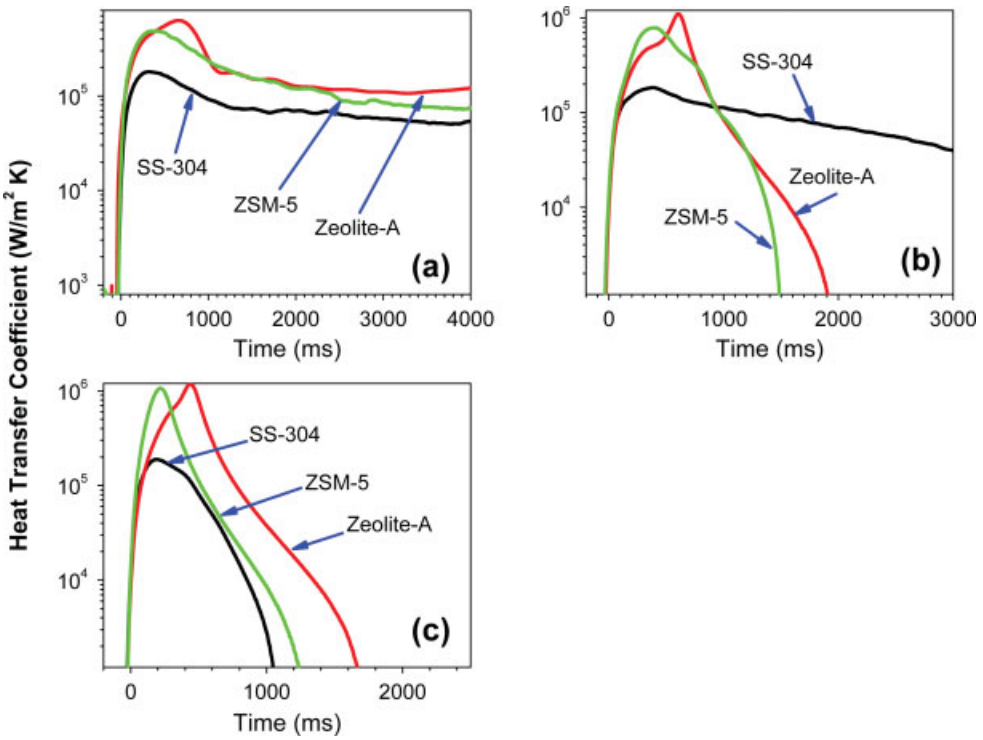

Figure 12. Heat transfer coefficient (*h*) variation with time for different surface initial temperatures T_0.

(a) T_0 = 130°C, (b) T_0 = 160°C, and (c) T_0 = 200°C. [Color figure can be viewed in the online issue, which is available at www.interscience.wiley.com.]

At T_0 = 160°C, the heat transfer performances (heat flux and heat transfer coefficient) for the Zeolite-A and ZSM-5 surfaces are close, as shown in Figures 10–12. It is also clearly demonstrated in Figure 6 that the boiling phenomena of a water droplet on both surfaces is similar, such as bubble size and wetting area.

At T_0 = 200°C, the ZSM-5 surface has the highest heat flux while the Zeolite-A has the highest heat transfer coefficient. A potential explanation for the observed phenomena is that the unobstructed micropores in the Zeolite-A coating are adsorbing water that is later removed by a process other than boiling.[27] A defining difference between the ZSM-5 and Zeolite-A coatings synthesized for the experiments is the existence of a structure directing agent (SDA) that occludes the ZSM-5 pores.[28] At lower surface temperatures the desorption process is relatively slow and the life time of the droplet is defined largely by the previously mentioned processes. At higher temperatures, the removal of the water within the micropores of Zeolite-A dominates the droplet's observed lifetime. Because additional heat is required to remove this water, the expected decrease in surface temperature as compared to ZSM-5 can be observed (Figure 10c). These competing mechanisms also explain why there is no significant decrease in the Zeolite-A droplets life time with increases in temperature beyond T_0 = 150°C (Figure 9), despite the fact that the SS-304 and ZSM-5 droplet life times are decreasing.

Conclusion

Both direct imaging analysis and calculated heat transfer parameters show that at any temperature above 100°C, both Zeolite-A and ZSM-5 have higher heat flux and heat transfer coefficient than that of SS-304. These coatings could have great potential for use in heat exchangers for significantly improved performance.

Acknowledgment

We acknowledge the financial support from the Strategic Environmental Research and Development Program of the Department of Defense (DoD/SERDP) and the California Space Institute.

Literature Cited

1. Kim G, Lee H, Webb RL. Plasma hydrophilic surface treatment for dehumidifying heat exchangers. *Exp Therm Fluid Sci*. 2002;27:1–10.
2. Kim HY, Kang BH. Effects of hydrophilic surface treatment on evaporation heat transfer at the outside wall of horizontal tubes. *Appl Therm Eng*. 2003;23:449–458.
3. Ren X, Li T, Zhao Q. Effect of surface treatment on flow boiling heat transfer coefficient in caso4 containing water. *Chinese J Chem Eng*. 2006;14:122–126.
4. Munoz R, Beving D, Yan Y. Hydrophilic zeolite coatings for improved heat transfer. *Ind Eng Chem Res*. 2005;44:4310–4315.
5. Hong K, Webb R. Performance of dehumidifying heat exchangers with and without wetting coatings. *J Heat Trans-T Asme*. 1999;121:1018–1026.
6. Turissini RL, Bruno TV, Dahlberg EP, Setterlund RB. Corrosion failures in plate heat exchangers. *Mater Perform*. 1998;37:59–61.
7. Jones D. Corrosion of central heating systems. *Eng Fail Anal*. 1997;4:179–194.
8. Narivs'kyi O. Corrosion fracture of platelike heat exchangers. *Mater Sci*. 2005;41:122–128.
9. Sakhnenko N, Kapustenko P, Ved' M, Zhelavskii S. Analysis of pitting resistance of stainless steels in hot-water supply systems. *Prot Met*. 1998;34:331–335.
10. Sakhnenko N, Kapustenko P, Ved' M, Zhelavskii S. Susceptibility of stainless steels to pitting corrosion in hot-water supply systems. *Russ J Appl Chem*. 1998;71:84–87.

11. Navinsek B, Panjan P, Milosev I. Pvd coatings as an environmentally clean alternative to electroplating and electroless processes. *Surf Coat Tech*. 1999;119:476–487.
12. Legg K, Graham M, Chang P, Rastagar F, Gonzales A, Sartwell B. The replacement of electroplating. *Surf Coat Tech*. 1996;81:99–105.
13. Kwangtaek H, Webb R. Wetting coatings for dehumidifying heat exchangers. *Hvac R Res*. 2000;6:229–242.
14. Cheng XL, Wang ZB, Yan YS. Corrosion-resistant zeolite coatings by in situ crystallization. *Electrochem Solid St*. 2001;4:B23–B26.
15. Beving D, McDonnell A, Yang W, Yan Y. Corrosion resistant high-silica-zeolite mfi coating—one general solution formulation for aluminum alloy aa-2024-t3, aa-5052-h32, aa-6061-t4, and aa-7075-t6. *J Electrochem Soc*. 2006;153:B325–B329.
16. Beving D, Yan Y. Corrosion resistant zeolite coatings: a general coating for aluminum alloys. *Abstr Pap Am Chem S*. 2004;227: U1550–U1550.
17. Mitra A, Wang Z, Cao T, Wang H, Huang L, Yan Y. Synthesis and corrosion resistance of high-silica zeolite mtw, bea, and mfi coatings on steel and aluminum. *J Electrochem Soc*. 2002;149:B472–B478.
18. Munoz R, Beving D, Mao Y, Yan Y. Zeolite y coatings on al-2024-t3 substrate by a three-step synthesis method. *Micropor Mesopor Mater*. 2005;86(1-3):243–248.
19. Hong KT, Imadojemu H, Webb RL. Effects of oxidation and surface-roughness on contact-angle. *Exp Thermal Fluid Sci*. 1994;8: 279–285.
20. Bernardin JD, Stebbins CJ, Mudawar I. Effects of surface roughness on water droplet impact history and heat transfer regimes. *Int. J Heat Mass Transf*. 1997;40:73–88.
21. Michiyoshi I, Makino K. Heat-transfer characteristics of evaporation of a liquid droplet on heated surfaces. *Int J Heat Mass Transf*. 1978;21:605–613.
22. Xiong TY, Yuen MC. Evaporation of a liquid droplet on a hot plate. *Int J Heat Mass Transf*. 1991;34:1881–1894.
23. Qiao YM, Chandra S. Experiments on adding a surfactant to water drops boiling on a hot surface. *Proc Royal Soc Lond Series a-Math Phys Eng Sci*. 1997;453:673–689.
24. Cui W, Chanda S, McCahan S. The effect of dissolving salts in water sprays used for quenching a hot surface, Part 1. Boiling of single droplets. *J Heat Transf-Trans Asme*. 2003;125:326–332.
25. Beck JV, Blackwell B, Clair C. *Inverse Heat Conduction: Ill-Posed Problems*. New York: Wiley, 1985.
26. Aguilar G, Wang GX, Nelson JS. Dynamic behavior of cryogen spray cooling: Effects of spurt duration and spray distance. *Lasers Surg Med*. 2003;32:152–159.
27. Stach H, Mugele J, Janchen J, Weiler E. Influence of cycle temperatures on the thermochemical heat storage densities in the systems water/microporous and water/mesoporous adsorbents. *Adsorp-J Int Adsorp Soc*. 2005;11(3-4):393–404.
28. Lobo R, Zones S, Davis M. Structure-direction in zeolite synthesis. *J Inclus Phenom Mol*. 1995;21(1-4):47–78.
29. Tunnell JW, Torres JH, Anvari B. Methodology for estimation of time-dependent surface heat flux due to cryogen spray cooling. *Ann Biomed Eng*. 2002;30:19–33.

Appendix: Algorithm of Inverse Heat Conduction (IHC)[29]

For the 1-D (Fig. A1) linear case of temperature-independent thermal properties, the governing equation can be written as:

$$\frac{\partial^2(T(x,t)}{\partial^2 x^2} = \frac{1}{\gamma}\frac{\partial T}{\partial t} \tag{A1}$$

where γ is thermal diffusivity. The following boundary and initial conditions are used,

$$-\lambda\frac{\partial T(x,t)}{\partial x}\Big|_{x=0} = q(t) \tag{A2}$$

$$T(x,t)|_{x=\infty} = T_o \tag{A3}$$

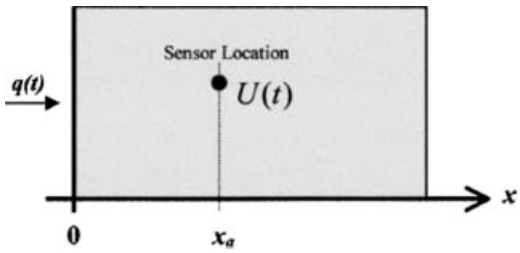

Figure A1. Schematic of the 1D heat conduction problem where the temperature measurements from a depth x_a are used to estimate the surface heat flux q (t).

$$T(x,t)|_{t=o} = T_o \tag{A4}$$

The measured internal temperature $U(t)$ can be written in index notion as

$$U_k = U(t_k) \quad k = 1,2,3.....k \tag{A5}$$

And the temperature distribution can be written as

$$T_{i,k} = T(x_i,t_k) \quad i = 1,2,3.....I \quad \text{and} \quad k = 1,2,3.....k$$

The surface heat flux is also expressed in a discrete form as

$$q_k = q(t_k) \quad k = 1,2,3.....k \tag{A6}$$

The values of heat flux at time t_1, t_2,..., t_K, represent the heat flux between times 0 to t_1, t_1 to t_2,..., $t_{K\text{-}1}$ to t_K, respectively.

The first step to solving this inverse problem is to represent the temperature distribution as a function of surface flux. We expand the temperature field in a Taylor series about the arbitrary but known values of surface flux q_k^* as

$$T_{i,k}(q_k) = T_{i,k}(q_k^*) + \frac{\partial T_{i,k}(q_k^*)}{q_k{}^*}(q_k - q_k^*) + \cdots \tag{A7}$$

The high order derivatives are zero. To simplify the problem, we introduce the following sensitivity coefficient:

$$Z_{i,k}^k = \frac{\partial T_{i,k}}{\partial q_k} \tag{A8}$$

Substituting Eq. A1 into Eq. A4 leads to

$$\frac{\partial^2 Z_{i,k}^k}{\partial^2 x^2} = \frac{1}{\alpha}\frac{\partial Z_{i,k}^k}{\partial t} \tag{A9}$$

$$-\lambda\frac{\partial Z_{i,k}^k}{\partial x}\Big|_{x=0} = 1 \tag{A10}$$

$$Z_{i,k}^k|_{i=\infty} = 0 \tag{A11}$$

$$Z_{i,k}^k|_{k=o} = T_o \tag{A12}$$

The sensitivity coefficient describes the temperature distribution within a medium due to a step response in surface

heat flux. Notice that the sensitivity coefficient is independent of the unknown surface heat flux. We calculate $Z_{i,k}^k$ numerically using an explicit central finite difference technique.

Assuming we know the temperature distribution and surface heat flux for times t_{k-1}, t_{k-2},... and that the surface heat flux at t_k is to be estimated, we can express the temperature field $t_{i,k}$ as a sole function of the unknown function of q_k. Substitute the sensitivity coefficient into Eq. A7, the temperature distribution can be expressed as

$$T_{i,k}(q_k) = T_{i,k}(q_k^*) + Z_{i,k}^k(q_k - q_k^*) \tag{A13}$$

In this case q_k^* is known from estimations at previous time, $Z_{i,k}^k$ can be calculated from Eqs. A9 to A12 and $T_{i,k}(q_k^*)$ is simply $T_{i,k-1}$. Equation A13 represents the temperature distribution as a sole function of surface heat flux q_k. Give that a temperature measurement is made in at least one location, for example, x_a, we introduce the measured temperature U_k into Equation A13 and solve for q_k

$$q_k = q_k^* - \frac{U_k - T_{i,k}(q_k^*)}{Z_{i,k}^k}, \quad i = a \quad k = 1, 2, 3.....k; \tag{A14}$$

However, the solution is severely ill-posed in that a small perturbation or noise in the recorded temperature can result in large oscillations in the predicted surface heat flux. To minimize the effects of measurement noise on the solutions, Beck[25] introduced the method of using future ($t > t_k$) temperature measurements where the surface heat flux is temporarily assumed constant over R future time steps:

$$q_k = q_{k+1} = ...q_{k+R} \tag{A15}$$

The least squares method is then used to minimize the error between the measured temperature U_k and the predicted temperature $T_{i,k}$ for a given sensor location (i.e., $x = x_a$) over future time steps

$$\Delta = \sum_{r=1}^{R} (U_{k+r-1} - T_{i,k+r-1})^2 \rightarrow min \quad i = a \quad k = 1, 2, 3.....k \tag{A16}$$

Since Eq. A13 can be used to calculate $T_{i,k+r-1}$ as a function surface heat flux, we substitute Eq. A13 into Eq. A16 to solve the least squares problem resulting in the solution for the estimated surface heat flux at time t_k:

$$q_k = q_k^* + \frac{\sum_{r=1}^{R} [U_{k+r-1} - T_{i,k+r-1}(q_k^*)] Z_{i,r-1}^k}{\sum_{r=1}^{R} (Z_{i,r-1}^k)^2}, \quad i = a \tag{A17}$$

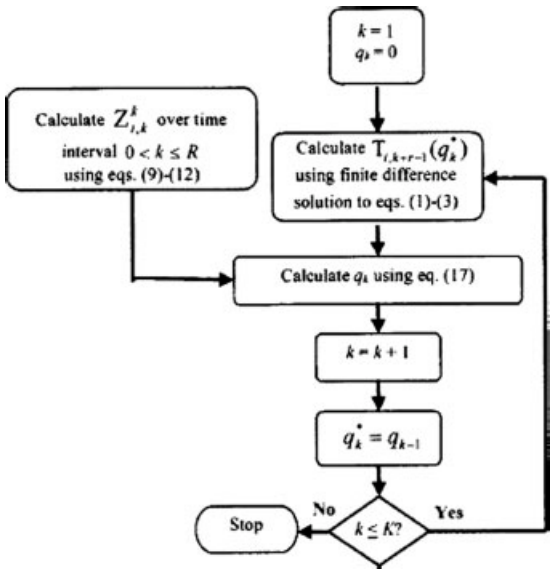

Figure A2. Flow diagram illustrating the algorithm to solve the inverse heat conduction problem.

Using Eq. A17, we sequentially solve for the surface heat flux for each time step. Figure A2 illustrates the complete solution methodology to the inverse heat conduction problem. Notice that $Z_{i,k}^k$ only needs to be calculated once for a given problem geometry since it does not depend on the unknown surface heat flux and is only calculated over the time interval $0 < t < t_R$. In addition, $T_{i,k+r-1}(q^*)$, $r = 1,2,...R$ can be calculated using a finite difference solution to Eq. A1 with the boundary conditions Eqs. A2 and A3, $q(t) = q^* = ...q_{k-1}$, and initial condition of $T_{i,k} = T_{i,k-1}$. Once the $T_{i,k}$ is calculated, the q_k can be obtained using Eq. A17.

Manuscript received Mar. 12, 2007, revision received Aug. 29, 2007, and final revision received Nov. 29, 2007.